Development and Test of C/C-SiC Combustion Chambers for Nitrous Oxide / Ethane Propellants in Space Propulsion

HEIDENREICH, Bernhard¹, JEMMALI, Raouf¹, TEIXEIRA, Hugo¹, CEPLI, Daniel¹, SMOLEY, Marco¹, Vogel, Felix¹, SEILER, Helge¹, ELSÄSSER, Henning¹, SELZER, Markus¹, PEICHL, Jonas¹, KURILOV Maxim², HÖRGER, Till², KIRCHBERGER, Christoph²

DLR – German Aerospace Center

¹ Institute of Structures and Design, Pfaffenwaldring 38-40, 70569 Stuttgart, Germany

² Institute of Space Propulsion, Lampoldshausen, Langer Grund, 74239 Hardthausen, Germany

Corresponding Author: Bernhard.Heidenreich@dlr.de
Email addresses: Raouf.Jemmali@dlr.de; Till.Hoerger@dlr.de; Maxim.Kurilov@dlr.de;
Cristoph.Kirchberger@dlr.de; Helge.Seiler@dlr.de; Jonas.Peichl@dlr.de; Henning.Elsaesser@dlr.de;
Markus.Selzer @dlr.de;

Abstract

In the frame of the DLR project "NeoFuels" novel thrusters, made of light-weight and high temperature stable ceramic matrix composites, have been developed for 20 N space propulsion systems. These so-called C/C-SiC materials are based on carbon fibres, embedded in a carbon and silicon carbide matrix, and are already commercially used for jet vanes in rocket propulsion as well as for high performance break discs in automobiles. The thruster design was based on a new, differential design, where the main components, i.e. nozzle, combustion chamber and interface, where separately manufactured in preform stage and joint together during the ceramization. The results from inner pressure tests of combustion chamber tubes and from the firing tests of thrusters, showed a high influence of the used carbon fibre type on the temperature and erosion resistance of the thrusters.

1 Introduction

For satellite propulsion, new propellants, offering a high performance, non-toxic, low cost and easy to handle green alternative to hydrazine are developed, worldwide. DLR is investigating several green propellants, among those are ADN (ammonium dinitramide) based propellants [1], hypergolic propellants based on hydrogen peroxide and ionic liquids [2] [3], nitromethane-based propellants [4], nitrous oxide/hydrocarbon mono- and bipropellants [5] [6][7][8][9] as well as hydrogen peroxide as monopropellant [10]. Across the globe, further alternatives as HAN-based (hydroxylammonium nitrate) propellants SHP-163 [11] [12] or AF-M315E (ASCENT) [13] [14] are investigated.

Another trend in space propulsion is maximizing the specific impulse Isp of propulsion systems. Usually, this also means that combustion temperatures also increase. To solve this issue, either costly high-temperature thruster materials, such as rhenium, iridium, or niobium, must be used, or regenerative cooling of the thruster must be implemented. In the case of monopropellants based on ADN or HAN, the former is usually employed, while the latter is used in N₂O/Hydrocarbon propulsion systems. While additive layer manufacturing (ALM) of metallic (Cu, stainless steel, titanium, niobium, inconel) thrusters has made implementing regenerative cooling easier, this manufacturing process remains complex. It requires rigorous monitoring of process parameters to ensure the required leak-tightness and surface quality in the cooling jacket and the plumbing system of the combustion chamber. Due to their small geometric size, this issue is especially severe in small thrusters (< 20 N). Additionally, regenerative cooling introduces an extra layer of complexity to propulsion systems, which is especially evident in off-design or intermittent operation [15][16][17][18].

C/C-SiC materials have been developed at DLR since the late 1980's [19] originally for the use in thermal protection systems for re-entry space vehicles. These materials are manufactured via the so-called liquid silicon infiltration (LSI), also developed at DLR. The LSI process can be subdivided in three main process steps. In the first process step, a CFRP (carbon fibre reinforced polymer) preform is manufactured by well-known manufacturing methods like

autoclave technique, warm pressing, filament winding or resin injection, using commercially available carbon fibres and polymer precursors with high carbon yield, for example phenolic resins. In the second process step, the CFRP parts are pyrolyzed at a maximum temperature of 1650 °C in inert atmosphere, leading to carbon fibre reinforced carbon (C/C) preforms. In the third and last process step, the C/C preforms are siliconized at 1650 °C in vacuum. Thereby, molten Si is infiltrated in the porous C/C by capillary forces and the SiC matrix is built up by a chemical reaction of Si and C, leading to a final C/C-SiC material, characterized by dense bundles of carbon fibre reinforced carbon (C/C) embedded in a silicon carbide (SiC) matrix. Structural parts with highly complex geometries are realized by joining of C/C subcomponents, manufactured separately. During siliconization, the subcomponents are converted to C/C-SiC and bonded together by a ceramic joint.

Due to the relatively fast process and the use of low-cost raw materials, LSI based CMC materials offer economic advantages compared to other, commercially used CMC manufacturing methods like chemical vapor deposition (CVI) or polymer infiltration and pyrolysis (PIP). Therefore, LSI based CMC's are the materials of choice for economically viable serial products like brake discs and pads for automobiles [20], high performance elevators [21] and the propeller brakes of aircraft [22]. Due to the unique combination of high temperature and thermal shock resistance with a low density (1.9 g/cm³), lightweight jet vanes for rocket motors could be developed successfully and transferred to industrial application [23].

In a new approach, the applicability of C/C-SiC materials for thruster structures have been investigated. Main objectives were:

- Light-weight and high temperature stable C/C-SiC thrusters for 20 N space propulsion systems using "laughing gas" liquid propellants, i.e. a mixture of nitrous oxide (N₂O) and ethane (C₂H₆).
- Development of high temperature resistant C/C-SiC material variants, enabling typical firing times from 0.1 seconds to 100 minutes per firing and total firing times of 30 minutes up to 10 hours.
- Design concepts for a cost-efficient manufacture of C/C-SiC thrusters, scalable to industrial production.
- Demonstrate applicability in real systems by hot firing tests of thrusters in original geometry.

A differential design approach has been introduced, which is offering technical as well as commercial advantages, compared to state-of-the-art manufacturing methods based on an integral, single part manufacture of thrusters, for example using filament winding or braiding processes [24][25][26][27][28]. The differential design is characterized by a dividing up of the thruster into basic elements (nozzle, combustion chamber (CC), interface flange). The CFP preforms of these elements are manufactured and pyrolyzed separately, machined and assembled in C/C stage, and finally joined during the siliconization process. Thereby different material variants, well adapted to the specific requirements of each element, can be combined in a single thruster. Additionally, efficient manufacturing methods can be used for the CFRP green body manufacture for each element.

2 Sample Manufacture

The mechanical and thermal testing of C/C-SiC material variants, preselected for the use in thrusters, was performed in four different steps:

- Inner pressure tests of C/C-SiC tubes
- Tension tests of short-fibre based plates
- Firing tests of combustion chamber liners and nozzle inlays
- Firing tests of thrusters

In order to determine the influence of fibre type and material composition on the mechanical properties and high-temperature stability, different C/C-SiC material variants, based on high tenacity (HT), intermediate modulus (IM) and ultrahigh modulus (UHM) carbon fibres (Table 1) were tested. Thereby endless fibres, 2D fabrics (2DF) and short fibres (SF; 1 fibre = 10 mm) were used, as well as different manufacturing methods (prepreg wrapping, warm pressing, autoclave technique, filament winding). C/C-SiC materials based on HT fibres are representing the standard material, widely used for TPS in spacecraft or brake components, and characterized by dense bundles of C/C and a high content of C matrix, leading to high strength and fracture strain, as well as to low densities and manufacturing costs. In contrast, the UHM-fibre based materials are characterized by a significantly higher and evenly distributed content of SiC matrix, offering higher abrasion and oxidation resistance, as well as higher thermal conductivity and raw material costs, compared to HT materials. In a third material variant, IM fibres, offering highest tensile strength and fracture strain, were used.

Fibre type		HT	IM	UHM
Fibre		HTA 40 E13	T800H	Granoc YS-90A-30S
Manufacturer		Tejin Tenax	Toray Composite Materials America	Nippon Graphite Fibres (NGF)
Fibre precursor		PAN	PAN	Pitch
Tensile strength	[GPa]	4.4	5.49	3.53
Young's modulus	[GPa]	240	294	880
Ultimate strain	[%]	1.7	1.9	0.3
Filament diameter	[µm]	7	5	7

Table 1 Mechanical properties of C-fibres.

2.1 Manufacture of sample tubes

Outer diameter

Fiber volume content in C/C

Open porosity in C/C-SiC

Ultimate tangential stress

Ultimate tangential strain

Density in C/C-SiC

Ultimate pressure

Standard deviation

Standard deviation

Standard deviation

Five different C/C-SiC tube variants (Ø 36 mm / Ø 40 mm x 200 mm) and (Ø 22 mm / Ø 28 mm x 150 mm) were manufactured by prepreg wrapping as well as by wet filament winding (Table 2). For the first method, so called prepregs were used, which are 2D fibre fabrics, impregnated with a liquid phenolic resin (JK 60), precured to a B-stage. Cut prepreg sheets were wrapped on a steel core and subsequently, the prepreg laminate was wrapped with a polymer shrink tape, which densified the lay-up during the heating up and curing in an oven. Densifying and curing of the different CFRP parts was performed at $T_{max.} = 220$ °C for two hours. The fibres were oriented in axial and circumferential direction (0°/90°), as well as in \pm 45°, due to the nature of the 2D fabrics.

The IM and UHM tubes manufactured via wet filament winding. Thereby, the fibre was impregnated with a liquid resin and wound on a rotating mandrel made of aluminium. A winding angel of \pm 54.7° relative to the tube axis was chosen, according to the net theory of fibre reinforced composites [29], considering the 2:1 ratio of tangential and axial stresses in a thin walled, closed tube under inner pressure. Subsequently the wound-up laminate was wrapped with shrinkage tape and cured in an oven. After curing, all the CFRP tubes were pyrolyzed, using graphite cores to support the CFRP tubes and to avoid distortion and delamination during the conversion of the polymer to the carbon matrix. After siliconization, the tubes were cut to length by abrasive cutting, using diamond coated tools.

C/C-SiC C/C-SiC C/C-SiC Material PR 288-5 R 391-393;402,4097,404, 411, 413, WR 361 WR 366 НТ НТ НТ IM UHM Sample tube $\pm 45^{\circ}$ $0^{\circ}/90^{\circ}$ $\pm 45^{\circ}$ $\pm 54.7^{\circ}$ $\pm 54.7^{\circ}$ Ø 22 Fiber type HTA 40 T800H YS 90 A Fiber preform fabric roving CFRP Manufacturing method Prepreg wrapping Wet filament winding 0°/90° ± 45° Fiber orientation [°] ±45° ±54.7 Inner diameter 35.8 35.5 [mm] 36.1 36.2 22.2

40.6

62.8

3.2

1.85

111.9

2.0

99.5

2.7

1.4

0.5

28.5

55.5

2.3

1.92

222.6

18.7

90.1

3.5

1.6

0.4

41.5

45.1

7.7

1.87

123.4

6.9

83.8

0.81

0.81

0.07

40.8

44.8

2.5

2.66

171.8

124.8

0.85

40.8

61.8

4.6

1.83

95.5

10.8

78.3

9.59

1.39

0.21

[mm]

[Vol.-%]

[%]

[g/cm³]

[bar]

[bar]

[MPa]

[MPa]

[‰]

[‰]

Table 2 Overview of materials for tube samples.

The fully automatized winding process ensures a reproducible quality of the resulting CFRP tubes. Due to the use of only one fibre roving, the manufacturing time for the winding up was quite long (8h) whereas for the winding up of the prepreg only a few minutes were needed. The main drawback of the prepreg wrapping is the use of costly prepregs, and the limited availability of prepregs with high performance fibres and suitable phenolic resins. Additionally, fibre orientation is restricted to $0^{\circ}/90^{\circ}$ or $\pm 45\%$, and therefore cannot be customized to the mechanical loads and stresses of the tube.

2.2 Manufacture of sample plates

The mechanical properties of three C/C-SiC material variants based on short fibres (SF) were determined by tension tests of coupons (120 x 20 x 4 mm³), cut out of SF sample plates (200 x 200 x 6 mm, Table 3). Thereby, different fibre types (HT, IM, UHM) cut to a fibre length of 10 mm, were mixed with dry, powdery phenolic resin JK63. The resulting press mass was filled into a press mould made of steel, and densified with a defined pressure cycle and a maximum pressure of 0.8 to 1 MPa. In parallel to the densification, the resin was heated up und cured with a defined heating cycle at a maximum temperature of 210 °C and pressed to the preliminary defined thickness. Thereby, maximum pressures of 4 to 6 MPa were applied. After pyrolysis and siliconization, the sample plates were grinded to accurate thickness and the coupons were cut out by abrasive cutting, using diamond coated tools.

		HT-SF	IM-SF	UHM-SF	
Fiber type		HTA 40	T 800H	YS 90 A	
Fiber preform	short fibers; fiber length 10 mm				
CFRP manufacturing method	warm pressing				
Fiber orientation	[°]	random			
Sample plate geometry	[mm]	200 x 200 x 6			
Fiber volume content in C/C	[Vol%]	47.5	46.9	40.6	
Open porosity in C/C-SiC	[%]	1.2	1.7	0.3	
Density in C/C-SiC	$[g/cm^3]$	2.04	2.12	2.50	
SiC content	[Vol%]	26	28	49	
C content	[Vol%]	64 64		47	
Si content	[Vol%]	10	8	4	
Tensile strength	[MPa]	34.8	33.1	65.9	
Standard deviation	[MPa]	5.0	6.22	7.56	
Tensile fracture strain	[MPa]	0.9	0.8	0.7	
Standard deviation	[MPa]	0.3	0.27	0.21	
Young's modulus	[GPa]	61.5	73.3	173.5	
Standard deviation	[MPa]	14.7	4.50	25.37	

Table 3 Overview of short-fibre based C/C-SiC SF materials.

2.3 Manufacture of thruster liners

For the testing of the material behaviour in a thruster relevant environment three different C/C-SiC combustion chamber tubes ($\varnothing 36 \text{ mm} / \varnothing 40 \text{ mm} \times 75.2 \text{ mm}$), based on HT fibres and prepreg wrapping, as well as on IM and UHM fibres, based on wet filament winding, were manufactured as described in 2.1. One short-fibre based nozzle liner (Figure 1) was manufactured using a CFRP preform plate $\varnothing 100 \text{ mm} \times 60 \text{ mm}$ manufactured by warm pressing of HT short fibres as described in 2.2 . After pyrolysis and siliconization, the tubes were cut to length and the outer

diameters of the tubes, as well as the entire contour of the nozzle inlay, were machined to ensure a close fit to the metallic combustion chamber.

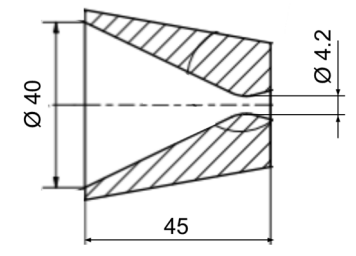


Figure 1 Design of C/C-SiC nozzle liner.

2.4 Thruster manufacture

For the thrusters (Figure 2, Table 4), nozzle segments were cut out of 2D-fabrics based C/C preform plates, manufactured by autoclave technique using 2D fabric prepregs. In a second approach, short-fibre based nozzles were manufactured close to the final geometry by warm pressing of the CFRP preforms (see 2.2.). For the combustion chamber, as well as for the interface flange elements, long tubes (200 mm) were manufactured by prepreg wrapping (see 2.1). After pyrolysis, the resulting C/C preform elements were cut out of the tubes and machined accurately at the interface areas, in order to provide a well-defined, tight fit between the corresponding joining surfaces. Subsequently, the joining paste, which was a defined mixture of phenolic liquid resin and carbon powder, was applied on all joining surfaces. The thruster elements were pressed together and the joining paste was cured in an oven. After the siliconization of the joint C/C thruster preform, the nozzle throat diameter, as well as the interface surfaces of the flanges were finally machined by dry grinding with diamond coated tools, in order to ensure an accurate assembly and a gas tight fit to the injector of the hot firing test facility.

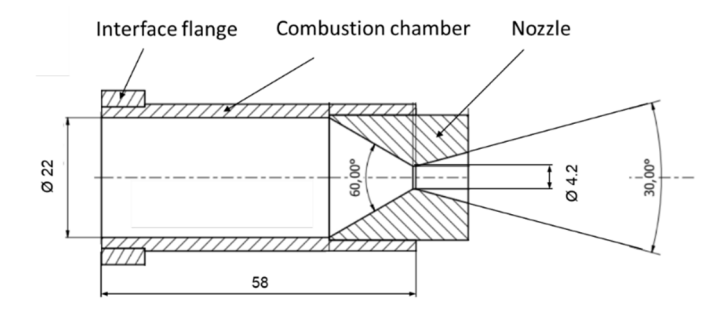


Figure 2 Design of C/C-SiC thruster Ø 22 / Ø 4.2 x 58

Table 4 verview of thruster samples.

Thruster type chamber / nozzle		нт / нт нт / инм		UHM / HT			
Thruster		T2	Т3	T4	T5	Т6	Т7
Combustion Chamber (CC)		НТА			UHM		
				2D fa	abric		
Nozzle		H ⁻	TA	YS	90	H.	TA
•			short	fiber		2D-f	abric
Interface Ring				H	ГА		
				2D fa	abric		•
Open porosity	[%]	3.2	3.8	1.4	-	2.4	2.0
Density	[g/cm³]	1.90	1.88	2.13	-	2.14	2.17

3 Sample Testing

In the first step of the development, sample liners for the combustion chamber and the nozzle were manufactured and tested in hot firing and inner pressure tests at room temperature. Promising material variants were selected for the manufacture of C/C-SiC thrusters in original size, which were again tested in hot firing and pressure test.

Porosity and density of the materials were determined via the Archimedes method (DIN EN 51918). The tubes and one thruster were tested under inner pressure, till fracture, using a manual hydraulic pump. Circumferential and axial strain of the tube samples were detected by strain gauges (Figure 3). The SF materials were characterized by tension tests of cut coupons (120 x 20 x 4 mm³) in a Zwick universal test machine.

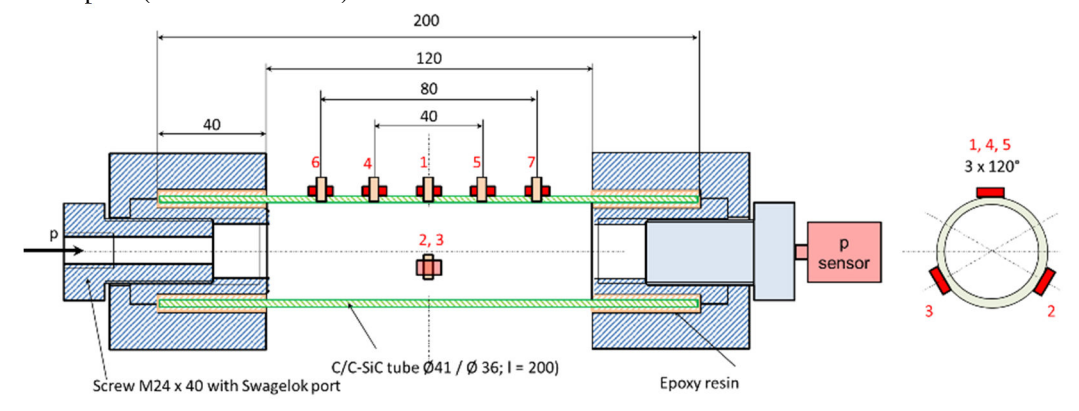


Figure 3 Test set up for inner pressure test, with the C/C-SiC tube Ø 36 mm glued into metal pressure connectors.

Micro computed tomography (μ CT) scans were performed using a high resolution μ CT system v|tome|L 240/450 (Baker Hughes, Wunstorf). X-ray parameters 200 kV/150 μ A, an exposure time of 334 ms and 1800 projections per sample were used to achieve a voxel size of 22 μ m. Data analysis and visualisation were conducted using the commercial software package VGStudioMax 2024.4 (Volume Graphics GmbH, Heidelberg).

Firing tests of C/C-SiC liners and thrusters were performed at the DLR Institute of Space Propulsion [30]. A green propellant based on nitrous oxide (N_2O) and ethane (C_2H_6) was used, enabling high theoretical combustion temperatures of up to 3 200 K. During the tests, maximum combustion temperatures between 2 600 and 3 200 K were expected. The test scenario was based on a typical 20 N propulsion system, with a nominal combustion chamber pressure between 6 and 9 bar. Nominal oxidizer-to-fuel (ROF) mixture ratio was 7 for the liners and 20 for the thruster tests, and was varied between 10.7 and 30 for the thruster tests. Characteristic length L* = combustion chamber volume / nozzle throat cross section was 7 m and 1.4 m for the liner and thruster tests, respectively. For the liner tests an already existing test set-up was used, which was designed for testing other propellants. The resulting, high L* was accepted for the preliminary testing. Firing time was 10 s for the first cycles and was increased stepwise to up to 60s.

The combustion chamber and nozzle liners were integrated in a modular test set-up made of a titanium-zirconium-molybdenum (TZM) combustion chamber and a massive copper nozzle, and tested in ambient atmosphere (Figure 4). The thrusters were connected to the injector using a flange interface and a graphite film sealant, and were tested in a vacuum test chamber ($V = 4 \text{ m}^3$; p < 3 mbar; Figure 5). The temperatures were measured with thermocouples, located with a distance of 1 mm to the inner diameter of the metal wall (CC liner), as well as on a defined position on the surface of the combustion chamber of the thrusters. Additionally, a thermo camera was used to get an overview of the temperature distribution of the thrusters, as well as to detect the high temperatures beyond the measuring range of the thermocouple (1 200 °C). The nozzle throat diameters were measured using test pins. A more detailed description is given in [30].

UHM/HT

10 - 60

		Firing time per cycle	Firing time total, max.	Pressure	ROF	Mass flux
		[s]	[s]	[bar]	[-]	[g/s]
Combustion chamber liner	НТ	10 - 90	190	7.8	7	9.3
	IM	10 - 60	100	7.8 - 8	5 - 7	7.5
	UHM	10 - 60	160	7.9 - 8.2	7.9 - 8	9.4
Nozzle liner	Cu	10 - 60	100	7.8 - 8	5 - 7	7.5
	HT	10 - 150	330	8.4 - 8.6	7 - 7.5	8.5 - 8.7
Thruster	нт/нт	10 - 60	66	7.5 - 9	17 - 30	9 -9.3
	HT/UHM	1 - 60	644	6 - 9.5	10.7 - 20	9.2 - 10.5

219

6.4 - 7.3 18 - 21.1 9.5 - 10

Table 5 Test parameters for the firing tests of liners and thrusters.

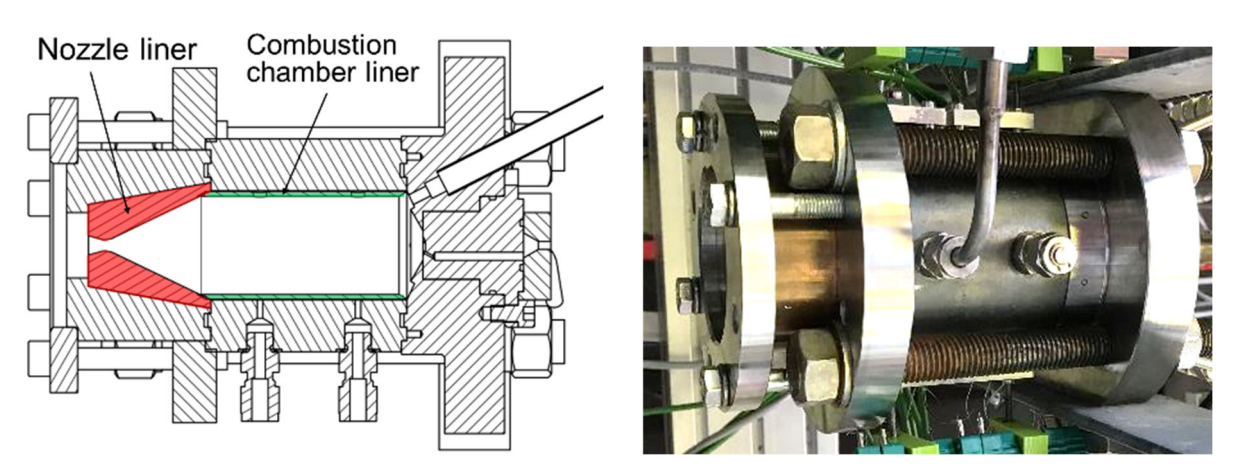


Figure 4 Test set-up for C/C-SiC combustion chamber and nozzle liner.

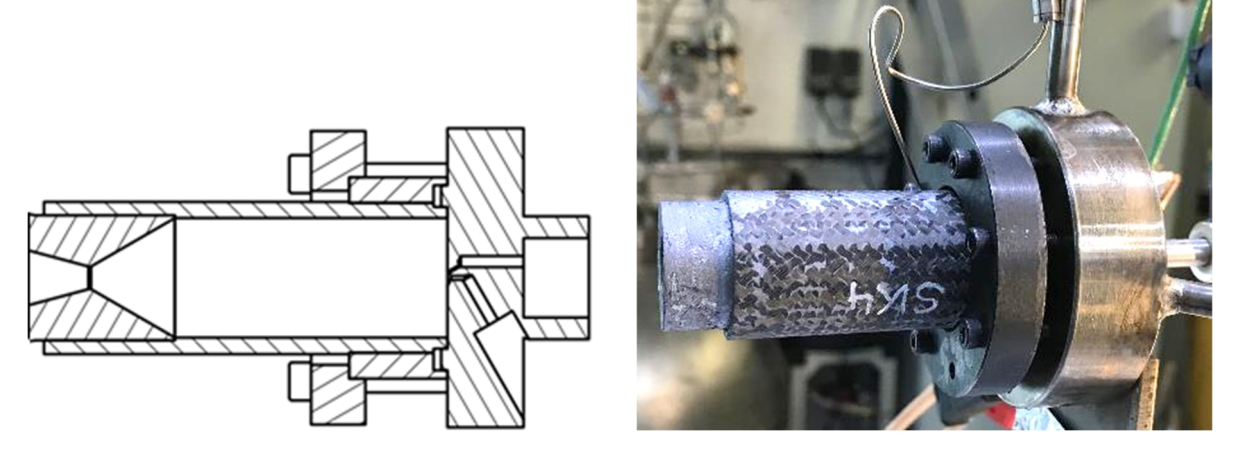


Figure 5 Test set-up for C/C-SiC thruster in the vacuum test chamber.

4 Results

4.1 Material test results

The density of the HT and IM-tubes was similar (1.83 and 1.87 g/cm³). The UHM tubes showed a 42 % higher density ($\rho = 2.66$ g/cm³), which was explained by the high conversion rate of C matrix and C fibres to SiC, which lead to a high SiC content. HT and IM-fibre based tubes showed dense C/C blocks and only a small amount of SiC, created mainly at the boundary of the C/C blocks, whereas the UHM tubes were characterized by an almost complete conversion of the C matrix to SiC (Figure 6).

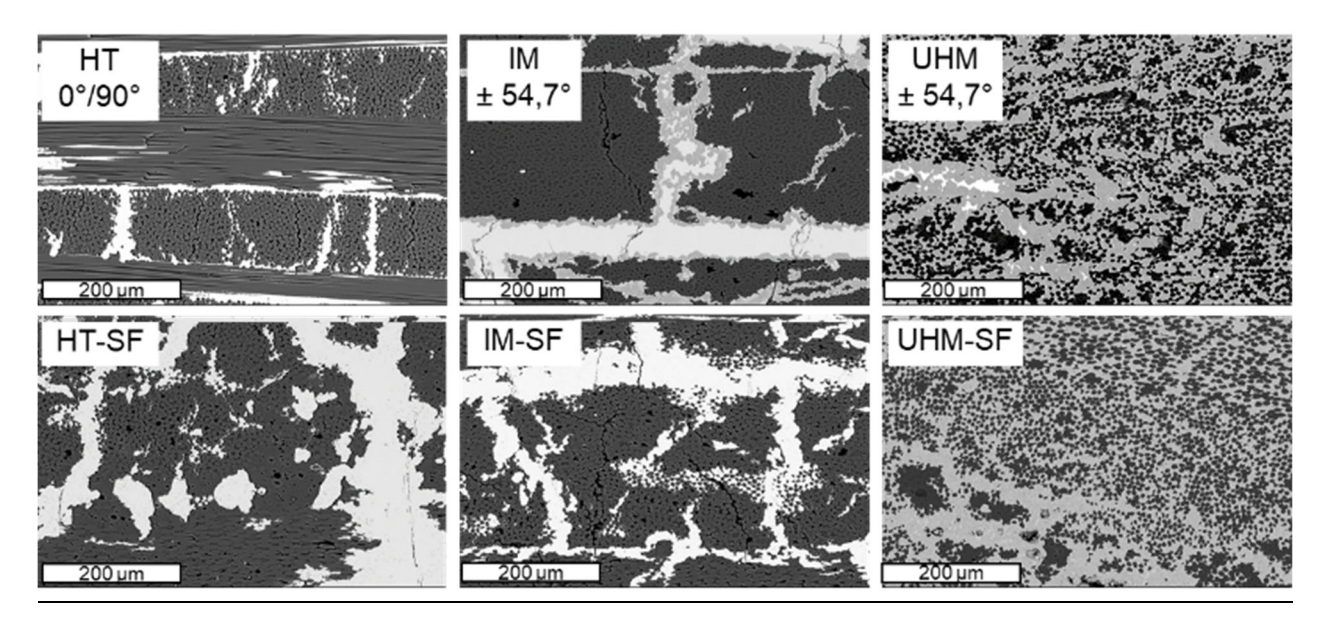


Figure 6 SEM images of the cross section of C/C-SiC materials based on fabrics and endless fibres (top), as well as on short fibres (bottom), showing the high content of C-fibres and matrix (dark grey) in the HT- and IM-materials, as well as the high SiC content (light grey) in the UHM materials. Residual Si (white) is visible in the centre of wide microcracks.

4.2 Inner pressure test results

The tube samples showed bursting pressures between 95 bar and 170 bar for the larger tubes (Ø 36) and 222 bar for the small tubes Ø 22 mm, as expected (Figure 7). The filament wound UHM tubes offered highest fracture strength of $\sigma_{max, UHM.} = 128.8$ MPa in tangential direction [31]. The fracture strength of the fabric-based HT tube with a fibre orientation of \pm 45 ° was 27 % higher compared to the 0°/90° tube, and even 18.7 % higher compared to the filament wound tube based on IM fibres ($\sigma_{max, IM} = 83.8$ MPa). By reducing the tube inner diameter from 36 mm to 22 mm, the fracture strength was only slightly reduced by 10 %. Fracture strain was highest for the HT tubes ($\varepsilon_{max.} = 1.4$ to 1.6 %) and lowest for the IM- and UHM tube ($\varepsilon_{max.} = 0.81 / 0.85$ %). This was explained by the lower fibre content and the higher conversion rate of the IM- and UHM materials, compared to the HT materials.

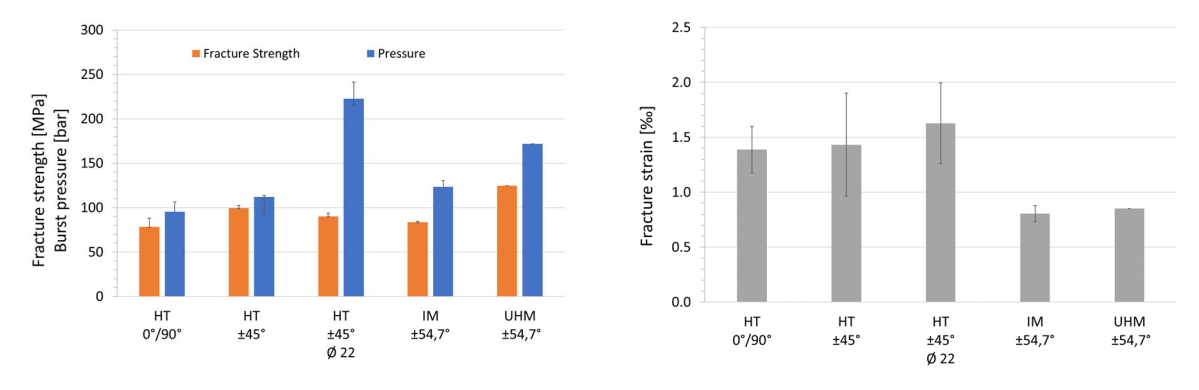


Figure 7 Bursting pressure, fracture stress and strain of the C/C-SiC sample tubes (see also [31]).

The short-fibre based C/C-SiC materials showed a lower strength level compared to the fabric or endless-fibre based tubes. Again, highest fracture strength was obtained by using UHM fibres ($\sigma_{max, UHM-SF} = 65.9 \text{ MPa}$), which was almost twice as high as for IM-SF and HT-SF. Highest fraction strain was obtained with the HT fibres (Figure 8).

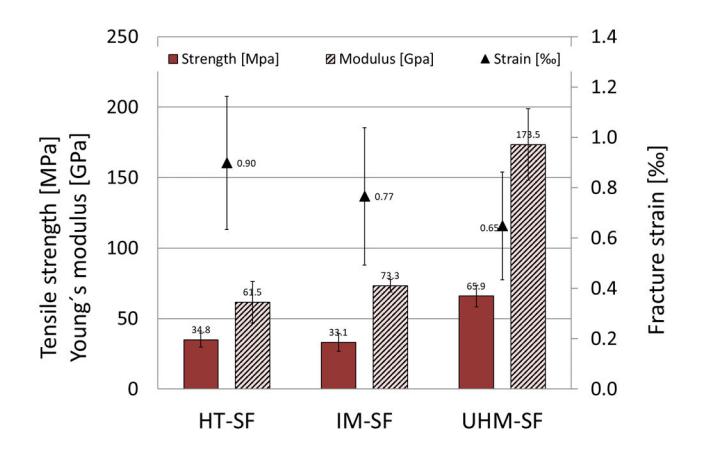


Figure 8 Mechanical properties of short fibre based C/C-SiC materials.

The HT/HT thruster failed by combustion chamber bursting at 173 bar (Figure 9). No failure of the joints between the combustion chamber and the flange or nozzle segment was observed.



Figure 9 HT/HT thruster in in inner pressure test set-up and after failure at 173 bar.

4.3 Liner test results

After 100 s of firing time, mass loss of HT and IM combustion chamber liner (0.89 ‰ and 0.83 ‰) was almost twice as high as for the UHM liner (0.46 ‰) (Figure 10). The abrasion of the Cu nozzle throat was quite high in the beginning, with a diameter increase of 50 μ m after the first test with only 10 s firing time, but no further abrasion was observed up to a testing time of 100 s (Figure 10). The C/C-SiC nozzle (HT-SF) showed a progressive increase of the throat diameter of up to 150 μ m after 330 s firing time. Comparing the increase of the nozzle throat cross-section area, which is relevant for L* and the efficiency of the thruster, the HT-SF nozzle liner offered a lower area increase as the copper throat, but showed a progressive area increase in the subsequent test cycles, due to the increase of firing time to 150 s in the last test cycle. However, after a cumulated test time of 330 s, the nozzle area increase was only 7.3 %, in total.

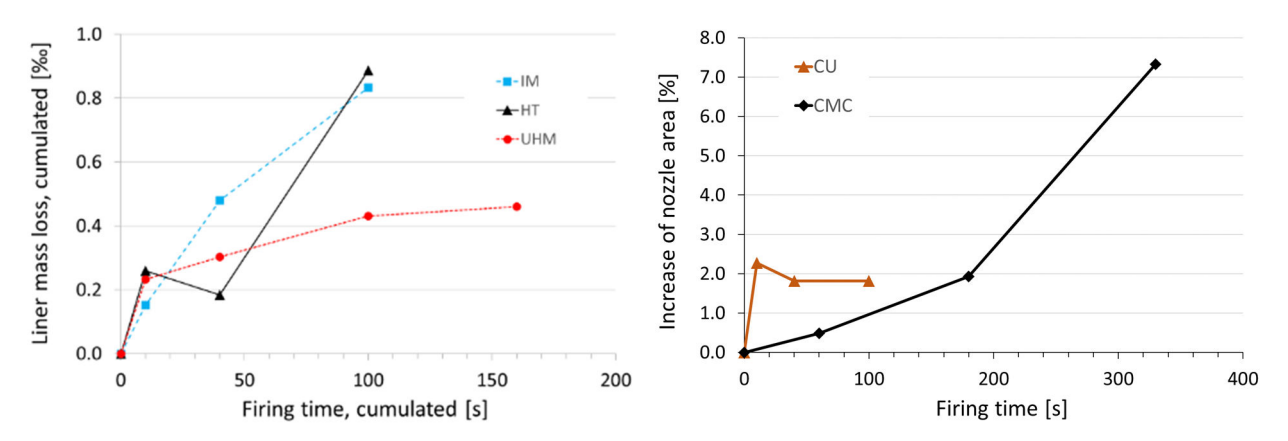


Figure 10 Cumulated mass loss and increase of nozzle cross-section area in dependence of firing time.

4.4 Thruster test results

All thrusters were tested until a burn-through of the combustion chamber wall was observed, indicated by a sudden decrease of combustion chamber pressure. All the joints between the combustion chamber and the nozzle as well as the flange were stable and no cracks, delamination or pull-out could be observed.

The maximum total firing time of 644 s was obtained with a HT/UHM thruster (T5; Figure 11). Pores and local delaminations in the combustion chamber walls of the HT/HT thrusters T2 (Figure 12) and T3 lead to lowest firing times of 66 s and 60 s, respectively. Despite the higher ceramic content in the combustion chamber walls of the UHM/HT thrusters, the total firing times were lower compared to HT/UHM thrusters. However, the failure mode was characterized by crack openings and small, longitudinal holes, in contrast to the extensive circular burn throughs in the HT combustion chamber (Figure 13). This effect could be traced back to microcracks, created in the combustion chamber tube already after the siliconization step. The microcracks were caused by the CTE mismatch between the UHM material of the combustion chamber and the HT material of the flange ring and the nozzle. Due to the higher SiC content of the UHM, the CTE was higher than for the HT material, characterized by the low SiC content and the dense C/C bundles, which lead to circumferential tension stresses in the combustion chamber tubes during the cooling down after siliconization, and finally to cracks in the joining area, proceeding axially in the entire length of the combustion chamber (Figure 14).

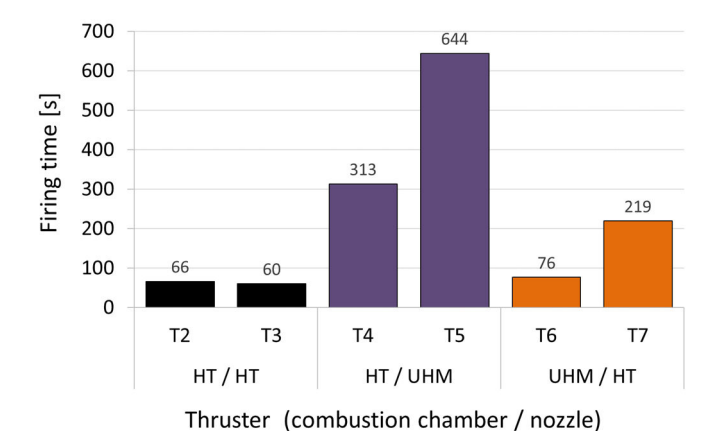


Figure 11 Maximum total firing time of the thrusters based on different materials.

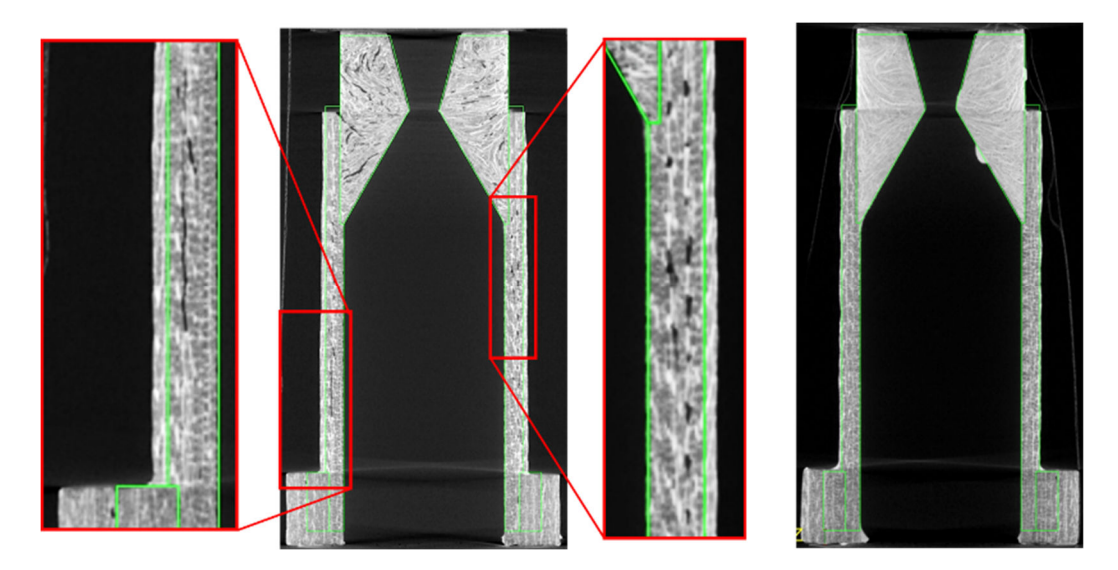


Figure 12 CT image of a HT/HT thruster T2 (left) with clearly visible pores and local delaminations in the combustion chamber wall. HT/UHM thruster T5 (right) with no pores visible.

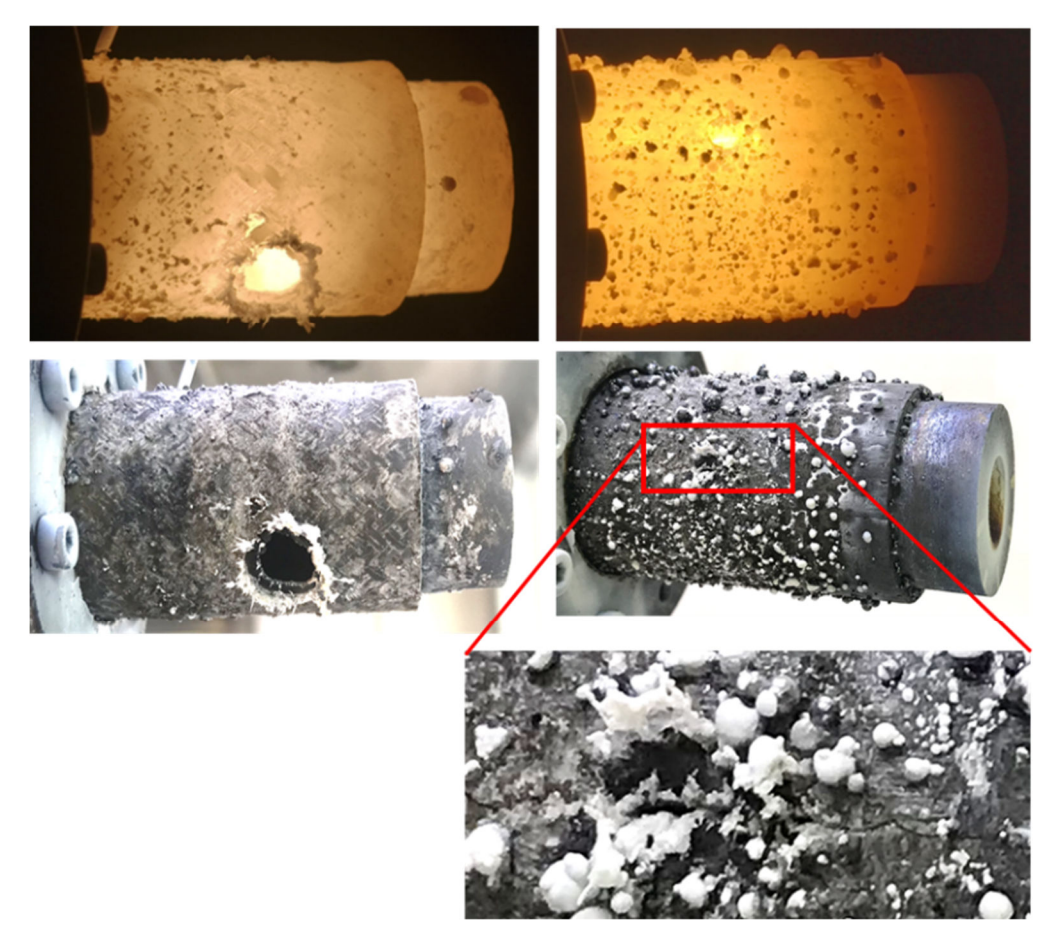


Figure 13 Extensive burn-through of thrusters with HT combustion chambers (T5, left) and typical crack opening failure of thrusters with UHM combustion chamber (T6, bottom).

During the firing, Si was melting, indicating a material temperature beyond 1 410 °C, the melting point of Si. Due to the pressure gradient in the combustion chamber, the Si melt was squeezed out of the material, formed droplets and splashed from the thruster outer surface. After the firing tests, the surface of the combustion chamber tube was covered with droplets of metallic Si and porous droplets of white coloured SiO₂, whereas inside the combustion chamber as well as in the nozzle throat, mainly SiO₂ was formed. The SiO₂ formation was confirmed by IR

spectrometer measurements. Due to the melting of SiO₂, maximum temperatures beyond 1 710 °C were estimated. Mass loss was lowest with the UHM / HT thrusters and highest for the thrusters with HT combustion chambers (Figure 15), which was again traced back to the higher SiC content of the UHM combustion chamber. The nozzle throat diameters of the HT-SF nozzles of T2 and T3 did not increase, but were almost blocked with Si and SiO₂, which was explained by the low firing time of 66 s. At longer firing times, the throat diameter increased to up to 16 % (T5). The HT nozzles based on 2D fabrics showed a higher, but more homogeneous increase of the diameter (Figure 16), whereas the short fibre based UHM nozzle lost his circular shape (Figure 17). However, the nozzles based on HT fabrics showed an oxidation of the C fibres and matrix at the nozzle throat, resulting in a porous structure of remaining SiC network. No increase of the nozzle throat area was measured for short firing times of HT/UHM (T4, 313 s) and UHM/HT (T6, 76 s) thrusters, but longer firing times showed the higher erosion stability of the UHM nozzle (Figure 18).

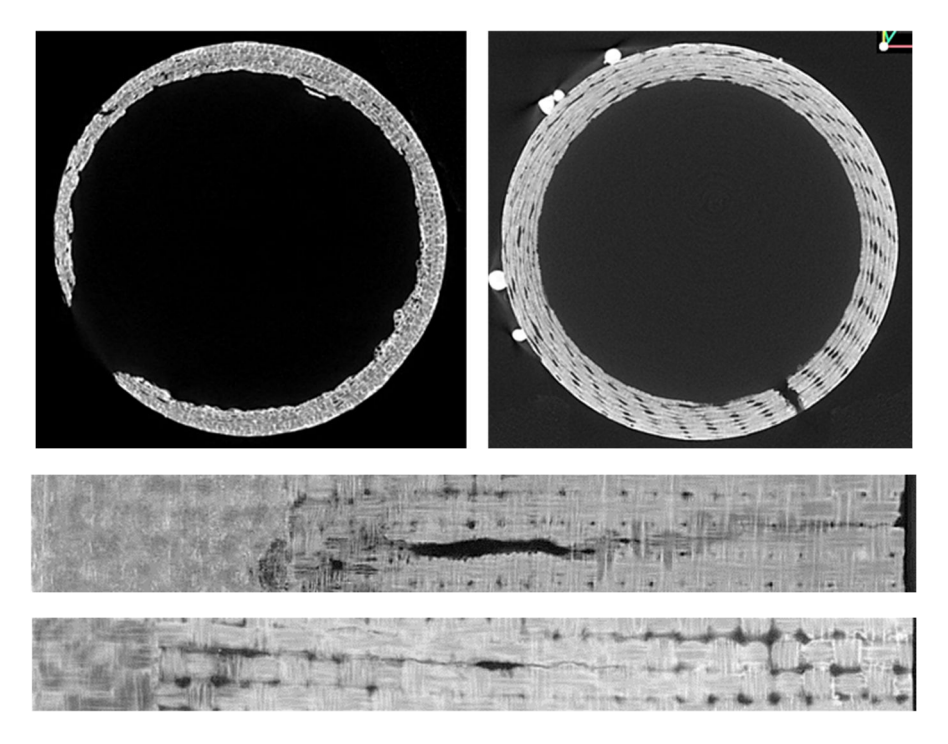


Figure 14 CT images of the combustion chambers after testing. HT chamber, showing erosion of wall thickness and large area burn-through (top left, T5), and UHM combustion chamber with low erosion of chamber wall, but local crack failure (top right, T6). CT images of UHM combustion chamber circumference (T6), showing a widening of the microcrack at the inner diameter (middle), compared to the narrow microcrack at the outer surface (bottom).

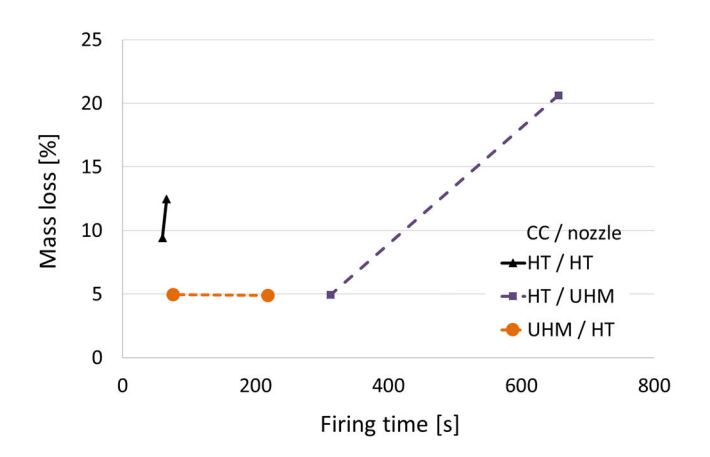


Figure 15 Mass loss of the thrusters after firing tests.



Figure 16 Nozzle throat diameters after firing, showing a stepwise erosion of the HT-2D nozzle surface, corresponding to the fabric lay-up, but a homogeneous increase of the diameter (left, T6). Less erosion but inhomogeneous increase of the UHM – SF throat diameter (T5) after 380 s (middle) and 644 s (right) firing time.

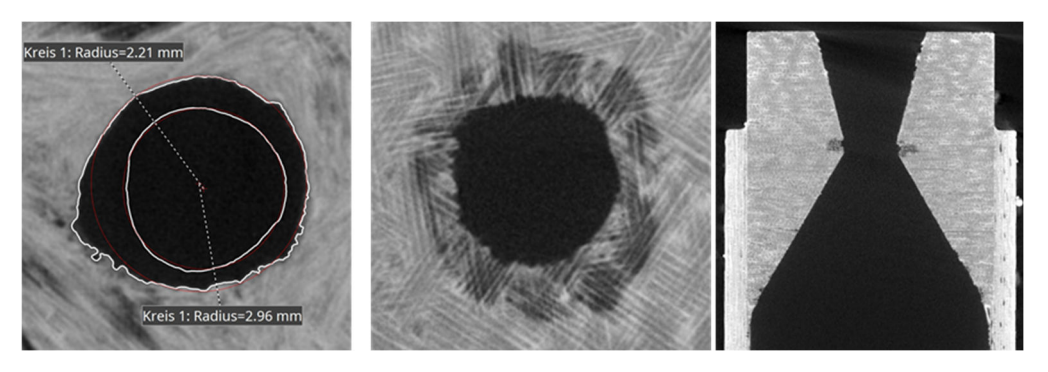


Figure 17 CT analysis of nozzle throat diameter of UHM SF (T5) before and after 644 s firing (left). Lower erosion of HT-2DF (T7) after 219 s firing (middle, right), but burning out of the C fibres and matrix at the nozzle throat.

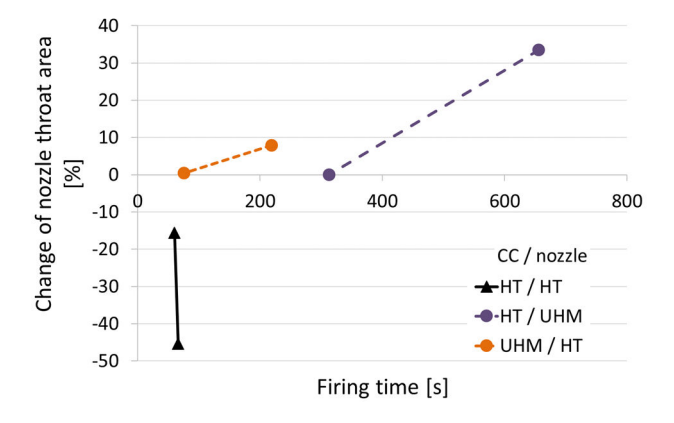


Figure 18 Increase of nozzle throat cross-section area of the tested thrusters.

5 Conclusion

C/C-SiC thrusters in the 20 N thrust class could be manufactured successfully by LSI and the feasibility of a new, differential design concept could be demonstrated. In hot firing tests, using N_2O / C_2H_6 as green propellant, a maximum burning time of ten minutes could be obtained with an uncooled C/C-SiC thruster, leading to maximum temperatures well beyond 1 700 °C at the outer surface of the thruster.

Due to the multi piece design approach, different C/C-SiC material variants and manufacturing methods could be combined in one single thruster structure. This offers a high potential for the development of environmentally stable thrusters with long operational lifetime, as well as for an efficient production of C/C-SiC thrusters in medium to large scale.

C/C-SiC material variants based on UHM fibres showed higher mechanical strength but lower fracture strain compared to HT and IM-fibre based material variants. Additionally, erosion stability of combustion chamber and nozzle throats was also highest for UHM variants, either based on 2D fabrics or short fibres. This was traced back to the higher, and more homogeneously distributed SiC phase content of the UHM-fibre based material variant.

The failure mode of UHM-fibre based combustion chambers was characterized by a burning through of microcracks, already existing before the firing tests, whereas the erosion of the chamber wall and the total mass loss of the thruster was low. Therefore, UHM based C/C-SiC material variants are favoured in general, and material combinations, ensuring crack free combustion chamber tubes will be in the focus of the future development.

Nozzles based on UHM short fibres showed a high erosion stability but uneven increase of the nozzle diameter, whereas HT materials using 2D fabrics lead to a favourable, homogeneous and circular increase of the nozzle diameter. Further tests are necessary to select the most convenient C/C-SiC material variant.

6 Outlook

The further development will be focused on minimizing the content of unreacted Si in the C/C-SiC materials, in order to avoid the forming of SiO₂ in the combustion chamber as well as the squeezing out and evaporating of Si and SiO₂. Thereby, it is expected to increase the temperature and erosion stability of the thruster and minimize the risk of contaminating surrounding payloads, when used in a satellite. This could be achieved by thermal or chemical removing of the Si, and replacing the Si by a ceramic matric, build up via polymer infiltration and pyrolysis. Cracks in the combustion chamber will be avoided by a more suitable combination of C/C-SiC material variants with similar CTE behaviour, or by introducing graded combustion chamber tubes.

In order to increase the erosion stability of the nozzle throat, the ceramic content will be increased by ceramic particle additives, homogeneously distributed in the short-fibre based press mass. Additionally, nozzles based on 2D UHM fibre fabrics will be tested, in order to combine the high erosion stability with the homogeneous, circular erosion behaviour.

Based on the promising results of this work, the development of a small 1 N thruster (Ø7 mm x 40 mm) for satellite propulsion was started in parallel. Thereby, also different design concepts (integral and differential), material variants and manufacturing methods will be in the focus.

7 References

- [1] M. Negri et al., "New technologies for ammonium dinitramide based monopropellant thrusters The project RHEFORM," Acta Astronautica, vol. 143, no. 1, pp. 105–117, 2018, doi: 10.1016/j.actaastro.2017.11.016.
- [2] M. Negri and F. Lauck, "Hot Firing Tests of a Novel Green Hypergolic Propellant in a Thruster," Journal of Propulsion and Power, pp. 1–11, 2022, doi: 10.2514/1.B38413.
- [3] F. Lauck, M. Negri, D. Freudenmann, and S. Schlechtriem, "Selection of ionic liquids and characterization of hypergolicy with hydrogen peroxide," Int J Energetic Materials Chem Prop, vol. 19, no. 1, pp. 25–37, 2020, doi: 10.1615/IntJEnergeticMaterialsChemProp.2019028004.
- [4] M. Kurilov, L. Werling, M. Negri, C. Kirchberger, and S. Schlechtriem, "Impact Sensitiveness of nitromethane-based green propellant precursors mixtures," in 8th Space Propulsion Conference 2022, 09-13. May 2022, Estoril, Portugal.
- [5] L. K. Werling et al., "Nitrous Oxide Fuels Blends: Research on Premixed Monopropellants at the German Aerospace Center (DLR) since 2014," in AIAA Propulsion and Energy Forum and Exposition, 2020. AIAA Propulsion and Energy Forum 24.-26.08.2020, 24.-26.08.2020.
- [6] Lukas Werling, "Entwicklung und Erprobung von Flammensperren für einen vorgemischten, grünen Raketentreibstoff aus Lachgas (N2O) und Ethen (C2H4): DLR-Forschungsbericht. DLR-FB-2020-39, 330 S," Dissertation, Institut für Raumfahrtsysteme, University of Stuttgart, Stuttgart, 2020.
- [7] T. Pregger et al., "Future Fuels—Analyses of the Future Prospects of Renewable Synthetic Fuels," Energies, vol. 13, no. 1, p. 138, 2020, doi: 10.3390/en13010138.
- [8] L. Werling and P. Bätz, "Parameters Influencing the Characteristic Exhaust Velocity of a Nitrous Oxide/Ethene Green Propellant," Journal of Propulsion and Power, vol. 38, no. 2, pp. 254–266, 2022, doi: 10.2514/1.B38349.
- [9] L. Werling and T. Hörger, "Experimental analysis of the heat fluxes during combustion of a N 2 O/C 2 H 4 premixed green propellant in a research rocket combustor," Acta Astronautica, vol. 189, pp. 437–451, 2021, doi: 10.1016/j.actaastro.2021.07.011

- [10]F. Lauck et al., "Test bench preparation and hot firing tests of a 1N hydrogen peroxide monpropellant thruster," in Space Propulsion Conference 14.-18.05.2018, Sevilla, Spain.
- [11] T. Katsumi and K. Hori, "Successful development of HAN based green propellant," Energetic Materials Frontiers, vol. 2, no. 3, pp. 228–237, 2021, doi: 10.1016/j.enmf.2021.09.002.
- [12] K. Hori, T. Katsumi, S. Sawai, N. Azuma, K. Hatai, and J. Nakatsuka, "HAN-Based Green Propellant, SHP163 Its R&D and Test in Space," Prop., Explos., Pyrotech., vol. 44, no. 9, pp. 1080–1083, 2019, doi: 10.1002/prep.201900237.
- [13] R. L. Sackheim and R. K. Masse, "Green Propulsion Advancement: Challenging the Maturity of Monopropellant Hydrazine," Journal of Propulsion and Power, vol. 30, no. 2, pp. 265–276, 2014, doi: 10.2514/1.b35086.
- [14] R. Masse, M. Allen, R. Spores, and E. A. Driscoll, "AF-M315E Propulsion System Advances and Improvements," in 52nd AIAA/SAE/ASME Joint Propulsion Conference, 25.-27. July 2017, Salt Lake City, Utah, USA, 2017.
- [15] Maleix, C., Chabernaud, P., Brahmi, R., Beauchet, R., Batonneau, Y., Kappenstein, C., ... & Scharlemann, C. (2019). Development of catalytic materials for decomposition of ADN-based monopropellants. Acta Astronautica, 158, 407-415.
- [16] Negri, M., Wilhelm, M., Hendrich, C., Wingborg, N., Gediminas, L., Adelöw, L., ... & Schwentenwein, M. (2018). New technologies for ammonium dinitramide based monopropellant thrusters—The project RHEFORM. Acta Astronautica, 143, 105-117.
- [17] Masse, R. K., Spores, R., & Allen, M. (2020). AF-M315E advanced green propulsion—GPIM and beyond. In AIAA Propulsion and Energy 2020 Forum (p. 3517).
- [18] Lukas-Buch: Werling, L., Lauck, F., Dobusch, J., Gritzka, M., Stratmann, V., Hörger, T., & Kirchberger, C. (2024). Mono-and Bipropellants Based on Nitrous Oxide and Fuels: State of the Art, Recent Developments in Academia and Industry, and a Special Focus on DLR's Activities. Recent Advancements in Green Propulsion: Green Propellants for Micropropulsion Systems, 161-186.
- [19] Krenkel, W. (2000). Entwicklung eines kostengünstigen Verfahrens zur Herstellung von Bauteilen aus keramischen Verbundwerkstoffen, Doctoral Thesis, Unversity of Stuttgart, DLR Forschungsbericht 2000-4.
- [20] Koehler, R. J. (2001) Manuscript of the presentation at the shareholders meeting of the SGL Carbon Group 2001, Germany.
- [21]Biffi, R., Zäch, B. (2002) Schindler 700 the Journey to the Top, Schindler Elevators, http://www.schindler.com/com/internet/en/media/press-releases-english/press-releases-2006-2000/schindler-700-the-journey-to-the-top.html.
- [22]B. Heidenreich, B., Zuber, C., Toro, S., Nardi, M. (2013) C/C-SIC Friction pads for an aircraft propeller brake, DGM Verbundwerkstoffe Karlsruhe 2013, Ed. A. Wanner/K.A. Weidenmann, ISBN 978-3-00-04230919, 19. Symposium Verbundwerkstoffe und Werkstoffverbunde, 03.- 05.07.2013, Karlsruhe
- [23] Verberne, O. (2006) Jet Vane Production Facilities Operational, Nammo bulletin 2006, www.nammo.com.
- [24] D. Ehmann, U. Gotzig, G. Schulte, S. Beyer, S. Schmidt, New European Apogee Motor Advanced Propulsion Technology, First Symposium on Potentially Disruptive Technologies and Their Impact in Space Programs, 7. April 2005, Marseille, France (2005).
- [25] S. Schmidt, S. Beyer, G. GahuZac, R. Meistring, M. Bouchez, Advanced ceramic matrix composite materials for current and future propulsion system applications, AIAA 2004-4019, 40th AIAA/ASME/SAE/ASEE Joint Propulsion Conference; Fort Lauderdale, Florida (2004).
- [26] C. Liu, J. Chen, H. Han, Y. Wang, Z. Zhang, A long duration and high reliability liquid apogee engine for satellites, Acta Astronautica 55 (2004), p. 401-408 (2004).
- [27] A. A. Kozlov, A. G. Vorobiev, I. N. Borovik, I. S. Kazennov, A. V. Lahin, E. A. Bogachev, A. N.Timofeev, Development Liquid Rocket Engine of Small Thrust With Combustion Chamber from Carbon - Ceramic Composite Material, in Nanocomposites with Unique Properties and Applications in Medicine and Industry, John Cuppoletti, Ed., ISBN: 978-953-307-351-4, http://www.intechopen.com/books/nanocomposites-with-uniqueproperties-and-applications-in-medicine-and-industry/development-liquid-rocket-engine-of-small-thrust-withcombustion-chamber-from-carbon-ceramic-composi (2011).
- [28] Andrea Wilson, Christopher Bostwick, Eric Besnard, Ceramic matrix composite as Liners for improved ablative chambers, 45th AIAA/ASME/SAE/ASEE Jpoint propulsion conference& Exhit, , Denver, Ohio, 2009
- [29] Altenbach, H. (2014) Holzmann/Meyer/Schumpich Technische Mechanik Festigkeitslehre, Springer Vieweg Wiesbaden, Ed. 11, https://doi.org/10.1007/978-3-658-06041-1.
- [30] Till Hörger, Bernhard Heidenreich, Maxim Kurilov and Christoph Kirchberger. Test analysis of C/C-SiC combustion chambers for nitrous oxide / ethane 22 N thrusters. 11th European Conference for AeroSpace Sciences (EUCASS) 30th June to 4th July 2025.
- [31] Heidenreich, B., Werling, L., Kurilov M., Kirchberger, C., Dauth, L., Lehnert, T., Elsäßer, H., Selzer, M., Seiler, H.; Development of CMC Combustion Chambers for Advanced Propellants in Space Propulsion, DOI: 10.13009/EUCASS2022-6114, 9th European Conference for AeroSpace Sciences (EUCASS), 2022.